GreenMemTraX: A User-Friendly Software for Super-Resolution Analysis of Membrane Protein Dynamics and Nanoscale Organization in Plants

Leander Rohr[1], Alexandra Ehinger[1], Luiselotte Rausch[1], Nina Glöckner Burmeister[2], Alfred J. Meixner[3], Klaus Harter[1], Birgit Kemmerling[1], and Sven zur Oven-Krockhaus[1,3,*]

1 Center for Plant Molecular Biology (ZMBP), University of Tübingen, 72076 Tübingen, Germany

2 Department of Biomedicine, Aarhus University, 8000 Aarhus, Denmark

3 Institute for Physical and Theoretical Chemistry, University of Tübingen, 72076 Tübingen, Germany

***Correspondence: Sven zur Oven-Krockhaus (sven.zur-oven-krockhaus@uni-tuebingen.de)**

ABSTRACT

Super-resolution microscopy provides deep insights into the dynamics of single membrane proteins and the nanoscale organization of plasma membrane proteins in living cells. However, in addition to plant-specific challenges in imaging applications, the elaborate analysis of single-molecule data complicates its widespread use in plant cell biological research. With GreenMemTraX, we provide a user-friendly, all-in-one, open-source software package that guides users through the steps of localization, tracking, mobility, and cluster analyses of plant plasma membrane proteins based on single particle tracking Photoactivated Localization Microscopy (sptPALM) data. GreenMemTraX dramatically simplifies data management following the FAIR (Findable, Accessible, Interoperable, Reusable) principles and increases the ease of use and reproducibility of the evaluated results. In addition, batch processing with detailed parameter output is available for all analysis paths, maintaining the consistency of raw data with the calculated results. The applicability of GreenMemTraX is demonstrated by evaluating sptPALM data for two representative plant plasma membrane proteins, namely the brassinosteroid receptor Brassinosteroid Insensitive 1 (BRI1) and the Receptor-Like Protein 44 (RLP44). Both were tested with the photoconvertible or photoactivatable fluorophores mEos3.2, PA-GFP, and PATagRFP and expressed in the *Nicotiana benthamiana* transient expression system and in stably transformed *Arabidopsis thaliana* plants. To facilitate plant applications,

GreenMemTraX provides a number of preset parameter settings to address plant-specific obstacles.

Keywords: GreenMemTraX, software, super-resolution microscopy, localization, single particle tracking, sptPALM, photoconvertible fluorophores, photoactivatable fluorophores, cluster analysis, plasma membrane proteins, BRI1, RLP44, plant

INTRODUCTION

The plasma membrane (PM) is one of the most important compartments, as it controls both homeostasis and mass transport and is the primary mediator of signals into or out of the cell. Most of these processes are controlled by membrane proteins. Analyzing their dynamics, organization and function is a fascinating area of research in plants and life sciences in general. Only a few techniques allow the in vivo analysis of membrane proteins with high spatiotemporal resolution. Suitable microscopy techniques include fluorescence recovery after bleaching (FRAP) (Axelrod et al., 1976; Peters et al., 1974), fluorescence correlation spectroscopy (FCS) (Magde et al., 1972), and single particle tracking (spt) (Manzo and Garcia-Parajo, 2015) of labelled membrane proteins, the latter being mainly driven by the advent of super-resolution technologies such as photoactivated localization microscopy (PALM) (Betzig et al., 2006; Hess et al., 2006). Application of sptPALM (Manley et al., 2008) is comparably underrepresented in plant cell biological research because of the structural peculiarities of plant cells having a cell wall.

Since sptPALM is a single-molecule microscopy technique, it depends on the detection of the fluorescence signal from individual fluorophores with sufficient contrast. This entails high demands on the imaging hardware and the brightness of the fluorophores. Commonly used very bright and stable fluorophores in animal cell biology, such as Alexa Fluor or Janelia Fluor dyes, pass through the PM into the cell and can be bound to proteins of interest using a variety of methods (Lelek et al., 2022). However, these organic dyes cannot pass the plant cell wall, so plant scientists predominantly rely on genetically encoded fluorophores fused to the proteins of interest. Consequently, the number of fluorophores usable for sptPALM in plant approaches is limited (Hosy et al., 2015; McKenna et al., 2019).

64 The best contrast for imaging membrane proteins is usually achieved in animal cells
65 under total internal reflection (TIRF) as their PM can be placed directly above the
66 coverslip. However, due to the additional, about 1 to 10 µm thick cell wall of plant cells,
67 the plant PM is not in the optimal range for TIRF (below 150 nm). Therefore, alternative
68 illumination methods such as highly inclined thin illumination (HiLo) (Tokunaga et al.,
69 2008) or variable angle epifluorescence microscopy (VAEM) (Konopka and Bednarek,
70 2008) must be used, which in turn have detrimental effects on the signal-to-noise ratio.

71 These technical difficulties have contributed to the fact that dynamic analysis of
72 membrane proteins in plant cells at very high resolution has only recently taken off
73 (Bayle et al., 2021; Gronnier et al., 2019; Hosy *et al.*, 2015; Jaillais and Ott, 2020;
74 Martiniere and Zelazny, 2021; McKenna *et al.*, 2019). With the improvement of
75 technical possibilities in microscopy and the increasing acceptance of single particle
76 tracking, other analytical methods such as cluster analysis of proteins in the PM of
77 plant cells are now coming into focus, which, in addition to dynamic parameters such
78 as diffusion coefficients, can also provide information on the spatial distribution of
79 proteins in cell membranes (Gronnier et al., 2017; Perraki et al., 2018; Smokvarska et
80 al., 2023).

81 Despite the progress made in recent years, the analysis of sptPALM data is a
82 complicated, multistep process. First, the positions of the individual labelled
83 membrane proteins in each image must be determined with high precision
84 (localization), followed by the assignment of localizations across multiple images to
85 trajectories (tracking). The mobilities or proportions of mobile/immobile proteins are
86 then calculated from the analysis of these trajectories. Subsequently, the number,
87 shape, and size of crowded regions in the membrane are determined based on the
88 localizations or the tracks (cluster analysis). Each of these steps actually represents a
89 separate area of research. Localization depends on physical camera parameters and
90 localization algorithms that must incorporate noise statistics for the low photon counts
91 typical of single-molecule microscopy. Tracking can be performed with a variety of
92 algorithms, and the chosen parameters have a large impact on the data evaluation,
93 representation and thus their interpretation. Mobility analysis is initially performed
94 using mean square displacement (MSD) plots (Qian et al., 1991). Still, this method is
95 not always applicable and is highly dependent on the parameters used. Combining
96 sptPALM data with cluster analysis is a relatively recent development; several

methods having advantages and disadvantages, leading to different data evaluation, representation and interpretation. This procedural complexity and challenges prevent broader application of super-resolution techniques such as sptPALM in plant cell biology.

Although practical guides have been published recently (Bayle *et al.*, 2021), there is still a lack of all-in-one and comprehensive software packages that guide the user through all analyses without excessive specialized knowledge. The available software is usually limited to or specializes in only one of the above sub-steps, with compatibility problems between the different solutions. Furthermore, the individual software modules are typically designed for broad use but are predominantly adapted to animal research. In addition, the large number of adjustable parameters require advanced bioinformatics and microscopy expert knowledge. Focusing on plant PM dynamics and organization allows concentrating on key parameters, for ease of use and transparency of the analyses.

In this work we present an all-in-one comprehensive open-source software package, named GreenMemTraX, guiding the scientist user-friendly and intuitively through the steps of sptPALM-based localization, tracking, mobility- and cluster analyses of membrane proteins in plant cells. Moreover, the storage of the sptPALM data and metadata follow FAIR (Findable, Accessible, Interoperable and Reusable) guiding principles (Wilkinson et al., 2016) for scientific data management and stewardship. We explored three genetically encoded fluorophores (mEos3.2, PA-GFP and PATagRFP) of different photophysical characteristics, highly suitable for sptPALM studies in living plant cells. The PA-GFP and PATagRFP pair also enable dual-color sptPALM applications in the future. The applicability of GreenMemTraX is exemplified with the temporal and spatial dynamics of two representative plant membrane proteins, the brassinosteroid receptor Brassinosteroid Insensitive 1 (BRI1) and the Receptor-Like Protein 44 (RLP44).

RESULTS

Design and properties of GreenMemTraX

Main principles

GreenMemTraX is run as an executable program or as an application in MATLAB (Mathworks). The entire code is available on GitHub for maximum transparency and the accompanying manual answers any analysis-specific questions (both will be published after peer-review). For each implemented main analysis step (location, tracking, cluster analysis) an extensive literature research was performed to identify and test the most suitable method or algorithm for GreenMemTraX. As already mentioned in the introduction, existing software applications usually focus on a specific part of the analysis, which is processed there in detail. For the integration into GreenMemTraX, we choose software modules that deliver robust results quickly and that have achieved good results in peer-reviewed evaluations (Chenouard et al., 2014; Nieves et al., 2023; Sage et al., 2019). The published codes were partially adapted to the requirements in GreenMemTraX; alternatively, new software code was written following the steps described in the respective publications (see below for details).

Localization

The sptPALM raw data usually consists of time series images that are saved as TIFF image stacks. Typical formats are 100x100 to 400x400 pixels (corresponding to 10x10 to 40x40 µm) with 2 000 to 10 000 images and a frame rate between 20 and 50 Hz. These parameters can vary depending on the specific experiment but are mainly governed by the optimal magnification of the imaging system for single molecule detection, the choice of the frame rate that achieves sufficient contrast, the size of the imaged PM region of interest, and the photophysical characteristics of the chosen fluorescent proteins (FPs). To better represent the biological variance, many short movies of a tracked membrane protein from a multitude of different cells are better than a few long movies of only a few cells.

In the first step, the fluorophore-tagged proteins are localized in each image with high precision using algorithms developed for super-resolution microscopy. For this purpose, we adapted the core of the SMAP software (Ries, 2020) for 2D localization only. Its algorithm for determining single molecule positions uses a robust maximum likelihood estimation (MLE) of Gaussian point spread function (PSF) models, which was shown to be very accurate (Sage *et al.*, 2019) and also uses the processing unit of a graphics card for outstanding processing speed. In addition, the fitter can also account for the pixel-specific noise of commonly used complementary metal-oxide semiconductor (CMOS) cameras. Starting in the first tab of the software, after

supplying the raw data files, the user can start the localization process for a list of files using default parameters (Figure 1A). An auxiliary window can be opened to check the performance of the algorithm on selected single images and adjust the parameters if necessary. At the end of the localization process, three histograms show (i) the PSF sizes, (ii) photons and (iii) localization accuracy for all detected and fitted fluorescence spots. These histograms can be used to check the quality of the raw data and exclude outliers from further analysis, for example, localizations with unusually large PSFs due to poor focusing or aggregation artefacts. After review and possible adjustment or removal of invalid data, the molecule positions can be passed on to the next analysis step.

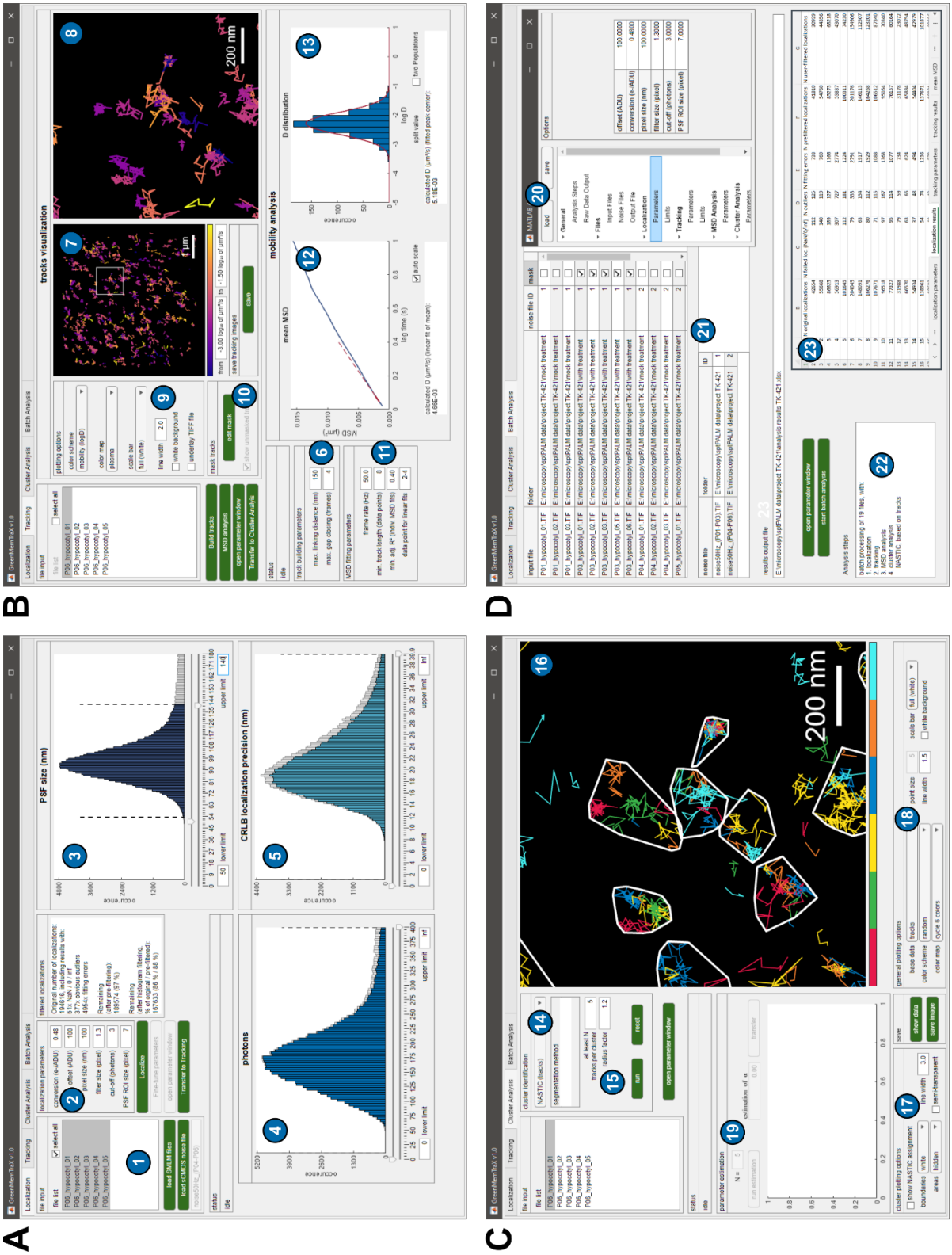

Figure 1. Graphical user interface of GreenMemTraX, with tabs for localization, tracking and mobility analysis, analysis of nanoscale organization and batch processing.

(A) Localization tab. After loading in the sptPALM files (1), the localization procedure is executed based on user-defined parameters (2), with its results visualized as three histograms (PSF sizes (3), photon numbers (4) and localization accuracy (5)) for all detected and fitted fluorescence spots. This serves as quality control and allows the user to filter out, e.g., badly localized single molecule positions. The selected files and their remaining localizations can then be transferred to the next tab, the **(B)** Tracking

178 tab. Here, the track building algorithm uses the specified parameters (6) to connect the detected
179 localization to trajectories, which are displayed in the overview image (7) and a user-defined magnified
180 view (8). Different layers and visualization options can be chosen (9), and the resulting images stored
181 as vector graphics. A binary mask can be defined for each file (10) to exclude tracks (for example, those
182 outside the cell area) from further analysis. The mobility analysis via MSD plots is also performed on
183 this tab, based on user-specified parameters (11), visualized as the mean MSD plot (12), averaging the
184 MSD data of the selected file(s), and the distribution of logarithmized, individual diffusion coefficients
185 (13), as a collection of derived diffusion coefficients from fitting the MSD curves of each individual track.
186 The fitting results representing the average diffusion coefficient are displayed below and might differ
187 considerably when multiple diffusive populations are present. Selected files can then be transferred to
188 the next tab, the **(C)** Cluster Analysis tab. The user can choose from several clustering algorithms (14)
189 and set their specific parameters (15). The visualization of the results (16) depends on the chosen
190 method and can be adjusted with several options (17), (18). For some algorithms, parameter estimates
191 can be calculated (19) based on the chosen data. **(D)** Batch Analysis tab. All user-specified parameters
192 from all previous tabs are stored in a systematic overview window (20) that can be opened from any
193 tab. Input files for batch processing are also added here and are shown as tables (21) for inspection
194 and the assignment of noise files and masks. The entire file list can then be automatically processed,
195 beginning with the localization procedure and may include tracking, mobility and cluster analysis as
196 chosen by the user, summarized in (22). All parameters and results are stored in a comprehensive
197 spreadsheet file, a section of which is shown as the inset (23). Additional options for all tabs are detailed
198 in the GreenMemTraX manual.

199 ***Tracking***

200 In the second tab of GreenMemTraX **(**Figure 1B**)**, the individual protein localizations
201 are linked through time to obtain trajectories or tracks. The generally low localization
202 density in sptPALM data allows for a simple but very fast tracking algorithm that can
203 also bridge detection gaps typical of single-molecule microscopy. The corresponding
204 code was adapted from a MATLAB program published by Jean-Yves Tinevez (Tinevez,
205 2011)**.** The principle of this simple Linear Assignment Problem (Simple LAP) tracker is
206 also part of his software TrackMate (Tinevez et al., 2017). After performing the
207 tracking, the resulting trajectories can be visualized (Figure 1B, upper plots), e.g.,
208 coloring them according to their duration, displacement, mobility and other
209 characteristics. In case of obvious connection errors, the tracking can be repeated with
210 adjusted track building parameters.

211 ***Mobility analysis***

212 The tracking tab of GreenMemTraX also provides mean square displacement (MSD)
213 analysis, which is the most widely used method for extracting diffusion coefficients and
214 motion patterns for this type of data (Manzo and Garcia-Parajo, 2015). A more detailed
215 description of this method was described by (Saxton and Jacobson, 1997). Only
216 selected tracks with a certain minimum length are forwarded for the analysis, removing
217 short track artefacts that originate predominantly from background fluorophores. The
218 mean MSD over all tracks is calculated and the diffusion coefficient estimated via a
219 linear fit (Figure 1B, lower left plot) that commonly only includes the first few points of
220 an MSD curve. While this type of ensemble analysis gives a first impression of protein

221 mobility, a more detailed analysis is additionally performed by calculating MSD curves
222 for each track, thus estimating individual diffusion coefficients for each detected
223 membrane protein. Their distribution can then be plotted as a histogram (Figure 1B,
224 lower right plot), revealing, among other things, the existence of subpopulations that
225 were hidden in the mean MSD plot. Due to the small number of data points for
226 individual tracks, a goodness-of-fit threshold value (the adjusted R^2) can be specified
227 for the linear fit to reject inconclusive results. In addition to storing the peak lg(D) value
228 for each file examined, the relative proportion of multiple populations can also be
229 estimated. Performing the MSD analysis adds new options to the tracking images,
230 such as coloring tracks based on their mobility or splitting them visually into mobile
231 and immobile tracks.

232 ***Cluster analysis***

233 While mobility analysis provides information about the dynamics of membrane
234 proteins, their spatial organization can also be obtained by cluster analysis based on
235 the single molecule data. This is performed in a separate tab of GreenMemTraX,
236 where various computational methods can be applied (Figure 1C). Voronoi tessellation
237 is performed as in the SR-Tesseler software (Levet et al., 2015) or in ClusterViSu
238 (Andronov et al., 2016). Other methods include density-based spatial clustering of
239 applications with noise (DBSCAN) (Ester et al., 1996) and the recently introduced
240 nanoscale spatiotemporal indexing clustering (NASTIC) (Wallis et al., 2023). So far,
241 however, no method has become firmly established in cell biological research, partly
242 because the size, shape, and density of membrane clusters could not be satisfactorily
243 validated by an independent technique. In addition, the above algorithms define cluster
244 sizes differently, making it difficult to provide absolute values for the cluster
245 dimensions. Nevertheless, comparative analyses of membrane protein organization
246 are possible when they are performed with the same method. When applying the
247 different clustering methods, the user can base the analysis on two different data sets:
248 (i) all localized fluorophore positions in the sample or (ii) the centroids of the assembled
249 tracks. Option (i) disregards the assignment of localizations to individual membrane
250 proteins, which can result in varying numbers of cluster points for each protein, while
251 option (ii) assigns each detected membrane protein to one cluster point, at the
252 expense of a smaller set of points. This choice largely depends on the available data
253 quantity, but option (ii) should be generally preferred for its more consistent
254 assignment. Only the NASTIC method is based solely on the protein tracks

255 themselves, since their spatial overlap is used for cluster analysis. GreenMemTraX
256 implements all the above algorithms, so the users can follow their preferences or
257 compare different algorithms. Again, the results of the applied analysis are visualized,
258 can be color-coded with different settings and exported for publication.

259 ***Batch processing***

260 The last tab contains the batch analysis (Figure 1D), which automatically processes
261 the raw sptPALM data selected by the user and then stores all analysis results in a
262 consistent format. A summary of all parameters used for the individual steps in the
263 analysis of the membrane protein of interest are listed in an intuitive selection
264 structure. If necessary, parameters can still be changed here, and the subsequent
265 batch analysis is performed based on these parameters collectively for all analysis
266 steps (localization, tracking, mobility and cluster analysis). The parameter list is also
267 attached to the collected results, so that all steps and settings can be traced back
268 according to the FAIR principle.

269 Fluorophores for in planta sptPALM analysis

270 The choice of suitable fluorophores is a crucial step in all fluorescence imaging
271 techniques. The requirements are even higher for single-molecule techniques
272 including sptPALM, as the signal of individual fluorescent molecules must be detected
273 with sufficient contrast. In plant cells, the rather impenetrable cell wall largely
274 precludes the use of organic dyes and quantum dots, so that genetically encoded FPs
275 must be used, which are fused translationally to the membrane protein of interest.
276 Conversely, FPs exhibit comparatively low photostability and brightness. Moreover,
277 sptPALM analyses of membrane proteins require photoactivatable or -convertible FP
278 variants, where the density of visible fluorophores per image is controlled by an
279 additional activation laser, further limiting the pool of applicable FPs. Genetic
280 constructs encoding photoconvertible mEos2 fusions have been useful for sptPALM-
281 based analyses of membrane proteins in plant cells (Gronnier *et al.*, 2017; Hosy *et al.*,
282 2015; Smokvarska *et al.*, 2023). However, (Zhang et al., 2012) showed that mEos2
283 has the disadvantage that it easily forms oligomers and aggregates when fused to
284 membrane proteins. We therefore implemented the improved version mEos3.2 that is
285 truly monomeric, is brighter, matures faster and displays higher photon budget and
286 label density (Zhang *et al.*, 2012). The native green form of mEos3.2 can be converted
287 to a red form using light of ~400 nm wavelength, allowing to adjust the density of the

288 visible fluorophores in the red imaging channel. However, as mEos3.2 occupies both
289 the green and red part of the spectrum, it is not compatible to combine it with other
290 FPs for potential dual-color applications. Based on their photophysical characteristics
291 (Table 1), we propose the use of photoactivatable (PA-) GFP (Patterson and Lippincott-
292 Schwartz, 2002) and PATagRFP (Subach et al., 2010) as additional fluorophores for
293 sptPALM applications in plant cells. Both PA FPs are non-fluorescent in their
294 respective native forms and can be converted to their spectrally distinct fluorescent
295 forms with light of ~400 nm, enabling simultaneous imaging of differently labelled
296 proteins in two color channels. The three fluorophore genes were codon-optimized for
297 their use in plant cells (Supplemental Table 1).

298 **Table 1. Basic spectral characteristics of the fluorophores mEos2, mEos3.2, PA-GFP and**
299 **PATagRFP.**

300 For the mEos fluorophores, both the native green (G) and the photoconverted red (R) form are listed,
301 while for PA-GFP and PATagRFP, only the activated forms are presented. A more detailed compilation
302 of their photophysical characteristics can be found in Supplemental Table 2.

	Excitation maximum (nm)	Emission maximum (nm)	reference
mEos2 (G)	506	519	(McKinney et al., 2009)
mEos2 (R)	573	584	(McKinney *et al.*, 2009)
mEos3.2 (G)	507	516	(Zhang *et al.*, 2012)
mEos3.2 (R)	572	580	(Zhang *et al.*, 2012)
PA-GFP	504	517	(Patterson and Lippincott-Schwartz, 2002)
PATagRFP	562	595	(Subach *et al.*, 2010)

303 ## Biological applications using GreenMemTraX

304 ### *Introduction of the intrinsic PM proteins used for proof-of-principle sptPALM analyses*

305 In order to demonstrate the applicability of GreenMemTraX for sptPALM analyses, two
306 well-described intrinsic membrane proteins were used, namely the brassinosteroid
307 (BR) receptor BRASSINOSTEROID INSENSITIVE 1 (BRI1) and the RECEPTOR-
308 LIKE PROTEIN 44 (RLP44).

309 BRI1 initiates well-understood signaling pathways in plant cells. Upon binding of BR
310 to BRI1's extracellular domain, its interaction with the co-receptor BRI1-ASSOCIATED
311 KINASE 1 (BAK1) is enhanced. This leads to a re-arrangement of proteins within the
312 complex, eventually resulting in auto- and transphosphorylation of their kinase
313 domains and its full signaling activity (Gou and Li, 2020; Wolf, 2020). The outcomes
314 of BR activation of the BRI1/BAK1 complex are on the one hand the differential
315 regulation of BR-responsive genes via a nucleo-cytoplasmic signaling cascade (Mora-

316 Garcia et al., 2004; Vert and Chory, 2006; Yin et al., 2005; Zhu et al., 2017) and on the
317 other hand a rapid acidification of the apoplast via the activation of PM-resident P-type
318 proton pumps (Caesar et al., 2011; Grosseholz et al., 2022; Witthöft et al., 2011)

319 RLP44 is proposed to be a cell wall integrity sensor that controls cell wall homeostasis
320 by interplay with BRI1 and BAK1 (Wolf et al., 2012; Wolf et al., 2014). In fact, we were
321 recently able to demonstrate the existence of a ternary RLP44/BRI1/BAK1 complex in
322 the PM of living plant cells using a spectral Förster resonance energy transfer (FRET)
323 and FRET-Fluorescence-lifetime imaging microscopy (FLIM) approach (Glöckner et
324 al., 2022). Additionally, RLP44 has been linked to phytosulfokine signaling. The
325 corresponding receptor Phytosulfokine Receptor 1 (PSKR1) is also proposed to form
326 a complex with RLP44 and BAK1 (Gomez et al., 2021; Holzwart et al., 2018).

327 ***GreenMemTraX analysis of BRI1 receptor dynamics and nano-structured organization***
328 ***in the Nicotiana benthamiana transient expression system***

329 For initial assessment, fluorescent fusion proteins were transiently expressed in
330 *Nicotiana benthamiana* (*N. benthamiana*) epidermal leaf cells. Transient expression
331 assays also provide robust results comparable with stably transformed Arabidopsis
332 lines as shown for the photoswitchable fluorophore mEos2 (Gronnier *et al.*, 2017;
333 Perraki *et al.*, 2018).

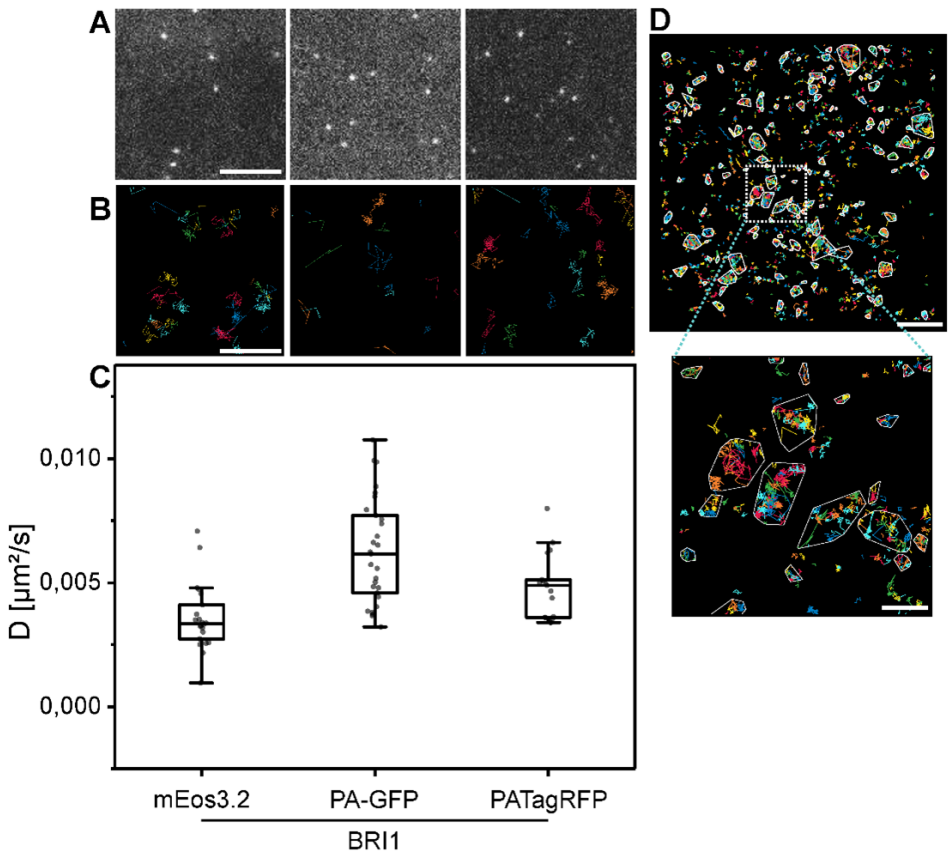

Figure 2. All BRI1-fluorophore fusions accumulate in the PM of epidermal cells of transiently transformed *Nicotiana benthamiana* leaves and their spatiotemporal properties can be analysed by GreenMemTraX.

(A) Representative images of sptPALM movies, showing, from left to right, single fusion proteins of BRI1-mEos3.2, BRI1-PA-GFP and BRI1-PATagRFP. The BRI1 fusion proteins were expressed via the native BRI1 promoter (*pBRI1*). Scale bar = 1 µM. **(B)** Representative magnifications of areas containing tracks generated by GreenMemTraX (random coloring per track) after localization of the BRI1 fusion proteins, with panels ordered as above. Scale bar = 100 nm. **(C)** Diffusion coefficients for the indicated BRI1 fusion proteins in the PM obtained with GreenMemTraX. For statistical evaluation, the data were checked for normal distribution and then analyzed applying the Kruskal-Wallis test followed by the Steel-Dwass post-hoc test, with n ≥ 17 for each fusion protein derived from at least six plants, measured on at least four different days. For detailed statistics see Supplemental Table 3. **(D)** The track data was used for cluster analysis in GreenMemTraX, exemplified by BRI1-mEos3.2 clusters that were assigned using the NASTIC algorithm. The top image represents one cell with random coloring per track and cluster boundaries highlighted in white. Scale bar = 2 µm. The bottom is a magnified view of the respective marked region in the top image. Scale bar = 500 nm.

Endogenous promotor driven constructs encoding the BRI1 and RLP44 fusions with the fluorophores mEos3.2, PA-GFP, and PATagRFP (see Materials) were transiently expressed in *N. benthamiana* epidermal leaf cells with the even distribution of activated fluorophores (Figure 2A) necessary for a comprehensive evaluation of sptPALM data (Bayle *et al.*, 2021).

Using GreenMemTraX (for detailed parameters see Supplemental Table 4), the data were processed, and trajectories generated (Figure 2B). After MSD analysis, the diffusion coefficients were calculated (Figure 2C).

358 Although the three fluorophores are sptPALM-optimized versions of different
359 precursors from various marine organisms, all three BRI1 fusion proteins showed
360 comparable diffusion coefficients in *N. benthamiana* epidermal leaf cells (Figure 2C).
361 This demonstrates that all three fluorophores can be reliably used for sptPALM studies
362 in plant cells. In live cell microscopy, the best signal-to-noise ratio was obtained with
363 mEos3.2, due to its excellent photophysical properties (Supplemental Table 2). On the
364 other hand, PA-GFP and PATagRFP can be combined - due to their non-overlapping
365 spectra - for dual-color sptPALM experiments.

366 As shown in Figure 2D, GreenMemTraX allows the use of sptPALM single-molecule
367 data to group BRI1 protein tracks into clusters.

368 In conclusion, we demonstrate that the transient expression system in *N. benthamiana*
369 is a suitable choice for testing mEos3.2, PA-GFP and PATagRFP fusions of PM
370 proteins in plant cells.

371 ***GreenMemTraX analysis of RLP44 dynamics and nano-structured organization in PM***
372 ***of transgenic in Arabidopsis thaliana***

373 To the best of our knowledge, neither mEos3.2 nor PATagRFP were used before for
374 sptPALM experiments in transgenic plants. In contrast, PA-GFP has been applied
375 previously (Martiniere et al., 2012; McKenna *et al.*, 2019).

376 For the generation of stable Arabidopsis lines via *Agrobacteria*-mediated
377 transformation, endogenous promoter (here *pRLP44*) constructs with the *RLP44*
378 cDNA and the codon-optimized versions of our fluorophores (see Methods) were used.

379 As shown in Figure 3A, all three RLP44 fusions successfully accumulated in
380 transgenic *Arabidopsis thaliana* (*A. thaliana)* hypocotyl cells in densities optimal for
381 sptPALM data evaluation. Using GreenMemTraX, trajectories were generated (Figure
382 3B) and the diffusion coefficients were calculated via MSD analysis. All three RLP44
383 protein fusions resulted in comparable diffusion coefficients (Figure 3C). We noticed
384 minor fluorophore-dependent differences in the RLP44 diffusion coefficients, likely
385 reflecting that the plant cells for the data sets may have had different cellular and
386 physiological stages.

387 All tagged RLP44 proteins allowed data processing suitable for cluster analysis using
388 GreenMemTraX (Figure 3D).

389 In summary, we demonstrate that mEos3.2-, PA-GFP- and PATagRFP-tagged
390 membrane proteins are suitable for sptPALM experiments in transgenic *A. thaliana*
391 and allow generation of data that can easily be analyzed by GreenMemTraX.

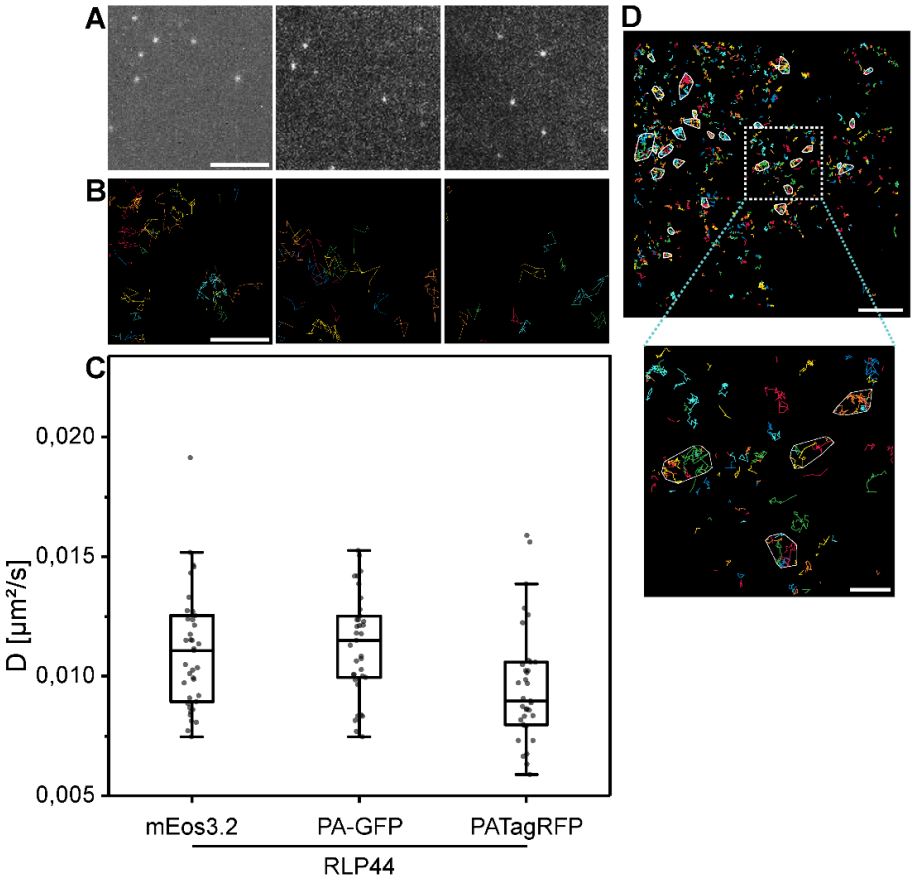

392

393 **Figure 3. All RLP44-fluorophore fusions accumulate in the PM of *Arabidopsis thaliana***
394 **hypocotyl cells and their spatiotemporal properties can be analyzed with GreenMemTraX.**

395 **(A)** Representative images of sptPALM movies, showing, from left to right, single fusion proteins of
396 RLP44-mEos3.2, RLP44-PA-GFP and RLP44-PATagRFP in the PM of hypocotyl cells of light-grown
397 *Arabidopsis* seedlings. The RLP44 fusion proteins were expressed via the native *RLP44* promoter
398 (*pRLP44*). Scale bar = 1 µM. **(B)** Representative magnifications of areas containing tracks generated
399 by GreenMemTraX (random coloring per track) after localization of the RLP44 fusion proteins in the
400 PM, with panels ordered as above. Scale bar = 100 nm. **(C)** Diffusion coefficients for the indicated
401 RLP44 fusion proteins calculated by GreenMemTraX. For statistical analysis, the data were checked
402 for normal distribution and then analyzed applying the Kruskal-Wallis test followed by the Steel-Dwass
403 post-hoc test, with n ≥ 35 for each fusion protein, from at least five plants, measured on at least three
404 different days. For detailed statistics see Supplemental Table 3. **(D)** The track data was used for cluster
405 analysis in GreenMemTraX, shown for RLP44-mEos3.2 clusters grouped by the NASTIC algorithm.
406 The top image represents one cell with random coloring per track, while cluster boundaries are
407 highlighted in white. Scale bar = 2 µm. The bottom image is a magnified view of the respective marked
408 region in the top image. Scale bar = 500 nm.

409 ***GreenMemTraX application examples to detect significant changes in protein mobility***

410 Most sptPALM analyses rely on comparing dynamic parameters of proteins, for
411 example, in response to environmental conditions such as hyper-osmotic stress
412 (Martiniere et al., 2019). We conducted sptPALM measurements in different light

413 conditions. GreenMemTraX-based data evaluation using transgenic *A. thaliana*
414 seedlings accumulating RLP44-mEos3.2 under the control of the *RLP44* promoter
415 (Figure 4) were performed in seedlings either grown in white light or darkness to
416 determine how the developmental state (photomorphogenic versus
417 skotomorphogenic) influences the dynamic properties of RLP44-mEos3.2 in the PM.
418 As shown in Figure 4A, RLP44-mEos3.2 moved significantly faster in in the PM of cells
419 of the upper part of dark-grown hypocotyls compared to the lower part. The diffusion
420 coefficient of RLP44-mEos3.2 in the PM of hypocotyl cells of light-grown seedlings,
421 where a differentiation of different cell types along the axis is hardly possible, was in
422 between the diffusion coefficients gained from the etiolated seedlings. These in planta
423 generated data show that tissue-specific differences of the RLP44-mEos3.2 dynamics
424 can be detected and analyzed by GreenMemTraX.

425 The effect of other environmental factors on protein mobility can also be evaluated by
426 GreenMemTraX. Here we chose the hyper-osmotic stress response of plant cells after
427 addition of sorbitol, a non-toxic, widely used, non-metabolic osmolyte already applied
428 for sptPALM (Hosy *et al.*, 2015). Sorbitol induces a clear cell volume loss (plasmolysis)
429 when used at a concentration of 300 mM. Under milder hyper-osmotic conditions
430 (100 mM), the cells experience a reduction in turgor without major changes in their
431 volume (Martiniere *et al.*, 2019). Thus, the increasing concentration of sorbitol from
432 100 to 300 mM induces a progressive separation of the PM from the cell wall which
433 changes the dynamics of almost all intrinsic PM proteins (Hosy *et al.*, 2015). Based on
434 this knowledge, treatments with 100 mM and 300 mM sorbitol or mock treatment were
435 performed with light-grown and dark-grown seedlings for 20 minutes. Then, the
436 sptPALM data for RLP44-mEos3.2 were measured in hypocotyl cells of light-grown
437 seedlings and cells of the upper hypocotyl of dark-grown seedlings and evaluated
438 using GreenMemTraX. Whereas the concentration of 100 mM sorbitol did not
439 significantly affect the diffusion coefficient of RLP44-mEos3.2 compared to the mock
440 treatment (0 mM), 300 mM sorbitol significantly increased its dynamic behavior in all
441 measured cells (Figure 4B).

442 These examples represent common analyses of sptPALM data in plant research, and
443 demonstrate the applicability of GreenMemTraX, which was used to perform all
444 analysis steps, including localization, tracking and protein mobility analysis.

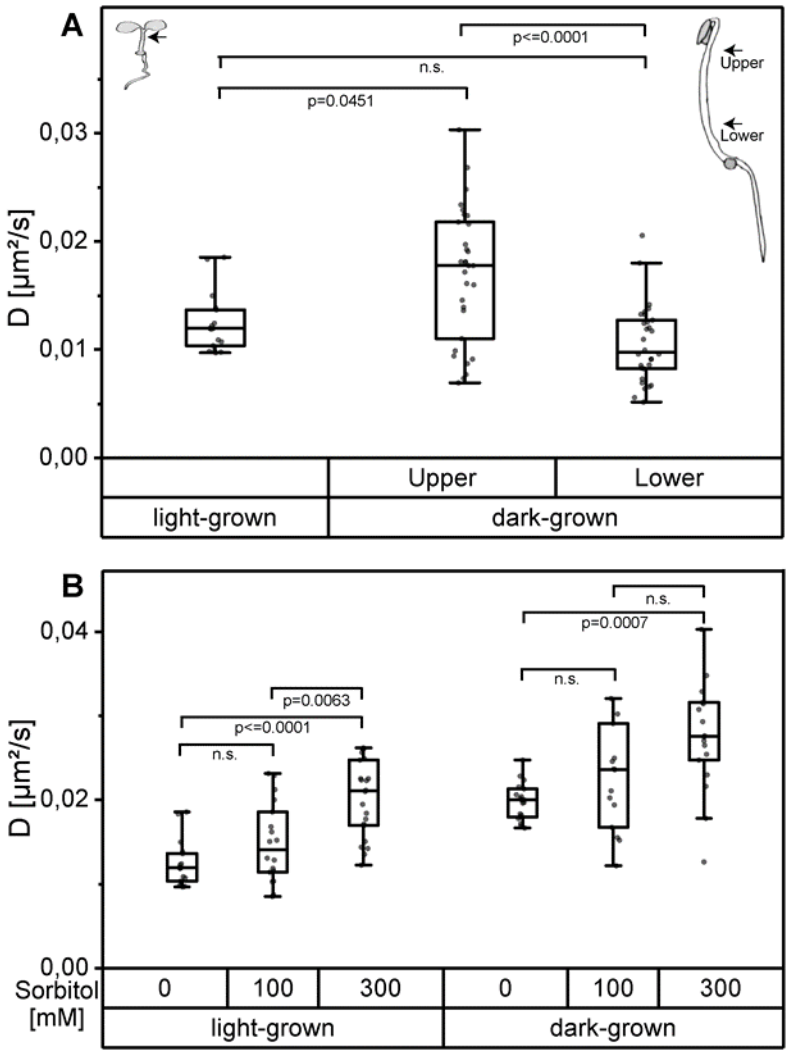

Figure 4. Evaluation of sptPALM data by GreenMemTraX reveals tissue-specific and environmental differences in the dynamics of RLP44-mEos3.2 in epidermal cells of the *Arabidopsis* hypocotyl.

(A) Diffusion coefficients of RLP44-mEos3.2 in epidermal hypocotyl cells of light-grown and dark-grown *A. thaliana* seedlings. The locations of the recorded measurements are indicated by arrows in the corresponding seedling sketches. For dark-grown seedlings, the center of the distance from the apical hook to the seed was used as the reference point. Based on this, the centers to the apical hook and to the seed were used as selected regions, named 'upper' and 'lower', respectively. For statistical evaluation, the data were checked for normal distribution and equal variances and the statistical analysis was performed using the Kruskal-Wallis test, with n ≥ 30, from nine plants, measured on three different days. For detailed statistics see Supplemental Table 3. **(B)** Diffusion coefficients of RLP44-mEos3.2 recorded from epidermal hypocotyl cells of light-grown or dark-grown *A. thaliana* seedlings after 20 min. treatment with sorbitol solution of 100 mM or 300 mM or mock-treatment (0 mM). For the recording of the data in the dark-grown seedlings the upper part of the hypocotyl cells was chosen (see (A)). For statistical evaluation, the data were checked for normal distribution. The statistical analysis was performed using the Kruskal-Wallis test followed by the Steel-Dwass post-hoc test, with n ≥ 14, from three different plants. For detailed statistics see Supplemental Table 3.

463 # DISCUSSION

464 ## GreenMemTraX is an all-in-one software package for sptPALM data
465 evaluation, optimized for plant cell biologists

466 With GreenMemTraX, we provide a user-friendly open-source software package that
467 guides users through the steps of localization, tracking, analysis of mobility and
468 nanoscale organization of membrane proteins on the basis of sptPALM data.
469 GreenMemTraX is tailored for use by cell biologists who want to perform sptPALM
470 analyses in plant cells. Due to the cell wall, only areas close to the microscope slide
471 can be analyzed in plants such as the plasma membrane and plasma membrane
472 associated proteins. This narrows down the large number of adjustable parameters
473 that are usually applied in sptPALM research in animal or human cell cultures and
474 tissues and will significantly lower the hurdle for sptPALM application in plant cell
475 biology.

476 GreenMemTraX has a default set of analysis parameters that is well suited for plant
477 PM proteins. However, all settings can be adjusted by the users to their specific
478 experimental requirements. Moreover, batch processing with detailed parameter and
479 data output is available for all analysis paths, maintaining the consistency of the
480 sptPALM data with the calculated results. The detailed but clearly structured
481 parameter organization also allows to investigate the influence of individual
482 parameters in the overall analysis process on the results, providing a method to
483 evaluate the reliability of the analyses. Importantly, the data management procedure
484 of GreenMemTraX follows the FAIR guiding principles for scientific data management
485 and stewardship. Due to its open-source characteristics, GreenMemTraX also allows
486 users to customize or extend the program according to their needs.

487 GreenMemTraX was programmed in MATLAB, a software language that is easy to
488 work with and widely used in academia. Care was taken to make the code
489 straightforward to understand and all programming steps are commented to make it
490 easier to insert changes or add extensions, which could also make GreenMemTraX
491 interesting for scientists working with animal or human cell cultures.

492 **PATagRFP, PA-GFP and mEos3.2 are suitable FPs for sptPALM analyses**
493 **in living plant cells**

494 The rather impenetrable cell wall almost completely excludes the use of organic dyes
495 and quantum dots for sptPALM applications in plant cells. Plant scientists therefore
496 rely on genetically encoded photoactivatable or photoconvertible FPs fused to the
497 protein of interest. With mEos3.2, PA-GFP and PATagRFP, three different FPs are now
498 available that do not aggregate, deliver satisfactory signal-to-noise ratios during
499 imaging and are therefore applicable for sptPALM applications both in a transient
500 transformation system (*N. benthamiana*) and in stably transformed *A. thaliana* plants.
501 We expect that these fluorophores will also work in other plant species. Of particular
502 interest is the combination of PA-GFP and PATagRFP, which will enable dual-color
503 sptPALM in the future for simultaneous recording and spatiotemporal analysis of two
504 different fusion proteins in the PM. Because of its superior photophysical properties,
505 we recommend the use of mEos3.2 for single FP fusion protein analyses. Especially
506 when using mEos3.2, but also the other FPs, the sptPALM technology shows its
507 superiority in terms of spatiotemporal resolution of membrane proteins in living plant
508 cells compared to other methods such as FRAP and FCS (Bayle *et al.*, 2021).

509 **GreenMemTraX allows the rapid in vivo analysis of membrane proteins in**
510 **transiently and stably transformed plant cells**

511 We used two functionally well-studied membrane proteins, namely BRI1 and RLP44,
512 for our proof-of-principle experiments regarding the usability of the three FPs and
513 applicability of GreenMemTraX. Both proteins were evaluated in either transiently
514 transformed *N. benthamiana* epidermal leaf cells or the epidermis of the hypocotyl of
515 stable transgenic *A. thaliana* seedlings. The accumulation of the BRI1 and RLP44
516 fusion proteins were driven by the respective endogenous promoters. Strong over-
517 accumulation of fusion proteins driven by constitutively active promoters leads to
518 overcrowded sptPALM movies. Analysis of these movies results in misconnected
519 tracks that affects the entire GreenMemTraX analysis causing inadequate results in
520 subsequent steps. Therefore, we recommend using weaker promoters whenever
521 possible.

522 GreenMemTraX offers different algorithms (Voronoi tessellation, DBSCAN, NASTIC)
523 for the analysis of the nanoscale organization of a given membrane protein. We

524 recommend the NASTIC algorithm as it is specifically designed to work with track data.
525 Because of the sensitivity to parameter changes, care must be taken when regarding
526 the results of the nanoscale evaluation output by all of these algorithms as absolute
527 values. However, relative comparisons of the nanoscale organization for a given
528 membrane protein are possible if there are no changes in the parameter settings
529 between the experiments.

530 GreenMemTraX captures developmental and physiological effects on the 531 in vivo dynamics of membrane proteins

532 During the GreenMemTraX analysis of the RLP44-mEos3.2 dynamics in epidermal
533 cells of light-grown *Arabidopsis* hypocotyls, we observed high data variability. This led
534 to the hypothesis that cell-specific effects depending on the cell's position in the organ,
535 i.e., on its developmental or physiological state, have an influence on the membrane
536 dynamics of the fusion protein to be investigated. This hypothesis was substantiated
537 by the technically easier access to the potential positional effects in the dynamics of
538 RLP44-mEos3.2 in epidermal cells along the hypocotyl axis of dark-grown seedlings:
539 The diffusion coefficient of RLP44-mEos3.2 is significantly higher in the epidermal cells
540 of the upper part than in those of the lower part of the dark-grown hypocotyl.
541 Furthermore, the diffusion coefficient in the lower part is similar to that found in the
542 epidermal cells of light-grown hypocotyls. GreenMemTraX can easily capture
543 differences in mobilities and allows sptPALM assays in different tissues that may vary
544 in their membrane properties.

545 As previously shown by (Hosy *et al.*, 2015; Martiniere *et al.*, 2019), the treatment of
546 *Arabidopsis* root cells with increasing concentration of the osmolyte sorbitol increases
547 the diffusion coefficient of membrane proteins such as aquaporins. Using
548 GreenMemTraX, we could confirm these findings and add potential effects of the
549 differentiation states of the analyzed tissue. This shows that reproducible and robust
550 data analysis is provided by our software tool.

551 In summary, sptPALM becomes more easily accessible and analyzable with
552 GreenMemTraX. The fluorophores mEos3.2, PA-GFP and PATagRFP have proven to
553 be suitable for sptPALM in planta and allow analysis of membrane proteins in transient
554 expression systems as well as in stable transformed plants. They are suitable for
555 treatment experiments and applicable in different tissues allowing also developmental

556 assays. The fast and easy evaluation of sptPALM data by GreenMemTraX will greatly
557 facilitate the comprehensive investigation of the dynamics and nanoscale organization
558 of membrane proteins in the future.

559 METHODS

560 Plasmid construction

561 All expression clones were constructed using GoldenGate assembly with BB10 as the
562 vector (Binder et al., 2014). Promoter sequences were obtained with the help of the
563 Integrated Genome Browser (Freese et al., 2016). Level I modules were generated by
564 PCR amplification of the desired sequences and then blunt-end cloned into pJET1.2
565 (Thermo Fisher Scientific). Fluorophores were designed as C-terminal fusions
566 (D-E module) using either a glycine/serine or a glycine/alanine rich linker. The coding
567 sequences of BRI1 and RLP44 were constructed as B-D modules, eliminating the
568 need for a B-C dummy module. A full list of used constructs can be found in
569 Supplemental Table 5. The correctness of Level I constructs was confirmed by Sanger
570 sequencing. Cut-ligations for the Level II generation were performed with 40 cycles,
571 without using bovine serum albumin as described by (Binder *et al.*, 2014). Reactions
572 were transformed into TOP10 cells (Thermo Fisher Scientific), and colony correctness
573 was verified via restriction enzyme analysis and partial Sanger sequencing.

574 Plant material and growth conditions

575 The transgenic *A. thaliana* lines used in this study were all in the Columbia (Col-0)
576 background. Stable lines were generated using the Floral dip method according to
577 (Zhang et al., 2006). Transgenic seeds were propagated either based on the presence
578 of the pFAST marker by binocular visual inspection or by selection of survivors on
579 ½ Murashige and Skoog (MS) plates containing 1 % (w/v) sucrose and 0.8 % (w/v)
580 phytoagar supplemented with 25 µM hygromycin. For sptPALM measurements, seeds
581 were sterilized with a solution of 70 % ethanol (v/v) and 0.05 % Triton X-100 for
582 30 minutes followed by a 10-minute treatment with absolute ethanol. Seeds were sown
583 on ½ MS plates (+1 % sucrose and 0.8 % phytoagar) and stratified at 4 °C for at least
584 24 hours. For measurements of dark-grown seedlings, seeds were exposed to light
585 from the growth chamber for two hours before being wrapped in aluminum foil until the

586 day of measurement. Light-grown seedlings were cultivated in growth chambers at
587 20 °C under long-day conditions (16 hours light / 8 hours dark). The duration of growth
588 is indicated in the respective figures. The *N. benthamiana* plants used in this study
589 were also cultivated under controlled conditions. Proteins were transiently expressed
590 using the AGL *Agrobacterium tumefaciens* strain (Lifeasible), as previously described
591 (Hecker et al., 2015; Ladwig et al., 2015), without the washing step with sterile water.
592 The plants were infiltrated with the respective construct at an OD600 of 0.1, in a ratio
593 of 1:1 with the silencing inhibitor p19. After watering, the plants were kept in ambient
594 conditions and were imaged three days after infiltration.

595 Sample preparation and movie acquisition

596 All sptPALM measurements with transiently transformed *N. benthamiana* were
597 performed three days after infiltration. A small leaf area was cut out, excluding veins,
598 and placed between two coverslips (Epredia 24x50 mm #1 or equivalent) with a drop
599 of water. This “coverslip sandwich” was then placed on the specimen stage, lightly
600 weighted down by a brass ring to help flatten the uneven cell layers, especially in
601 *N. benthamiana*. Seven-day-old *A. thaliana* seedlings were used to acquire data from
602 stable *Arabidopsis* lines. Depending on the experiment, either light-grown or dark-
603 grown plants were used. Similar to the handling of *N. benthamiana* leaf discs, the
604 seedlings were placed between coverslips and brass rings.

605 The custom-built microscope platform for sptPALM acquisition is described in detail in
606 the Supplemental Information. Briefly, lasers of different wavelengths and their
607 intensities are controlled by an acousto-optic transmission filter. A laterally translatable
608 lens in the excitation beam path allows to adjust the VAEM illumination of the sample
609 utilizing a high NA objective. The emitted light from the sample is separated from the
610 excitation light by a multi-band beam splitter and is detected by an sCMOS camera.
611 Depending on the fluorophore fusion, the following filters were inserted into the
612 emission beam path: (i) mEos3.2: 568 LP Edge Basic Longpass Filter, 584/40 ET
613 Bandpass; (ii) PA-GFP: 488 LP Edge Basic Longpass Filter, 525/50 BrightLine HC;
614 (iii) PATagRFP: 568 LP Edge Basic Longpass Filter, 600/52 BrightLine HC (all AHF
615 analysentechnik AG). The excitation power arriving at the sample was measured
616 (PM100D with S120C, Thorlabs) in epifluorescence mode after the objective to keep
617 it constant for the respective experiment sets. If necessary, photoconversion or

618 photoactivation was performed using 405 nm excitation at varying low intensities (for
619 detailed acquisition parameters see Supplemental Table 4). The magnification of the
620 optical system was adjusted so that the length of one camera pixel corresponds to
621 100 nm in the sample plane. Viable regions of interest were screened in a larger area
622 of 51.2 x 51.2 µm by adjusting the focal plane and the VAEM angle with a frame rate
623 of 10 Hz, while recording was performed with 12.8 x 12.8 µm and frame rates between
624 20 and 50 Hz, recording between 2 500 and 5 000 frames per movie (see
625 Supplemental Table 4). For each measurement day, noise files (a series of dark
626 images) were recorded with the corresponding frame rates.

627 **Raw data processing and analysis with GreenMemTraX**

628 Subsets of each experimental data set were loaded into GreenMemTraX to inspect
629 the quality of the data and to find appropriate parameters for each analysis step as
630 described above. On the Batch Analysis tab, all sptPALM raw data files that share the
631 same parameter set were processed together (see Supplemental Table 4 for a detailed
632 list of applied analysis parameters). Samples that showed significantly low numbers
633 of localizations or tracks compared to others in the same batch were discarded.

634 SUPPLEMENTAL INFORMATION

635 Document S1. Supplemental information.

636 FUNDING

637 Our research was supported by the German Research Foundation (DFG) via the CRC
638 1101 to A.J.M., B.K., K.H. and S.z.O.-K., and by individual DFG grants to K.H. (HA
639 2146/22, HA 2146/23). We also thank the DFG for grants for scientific equipment
640 (FUGG: INST 37/991-1, INST 37/992-1, INST 37/819-1, INST 37/965-1).

641 AUTHOR CONTRIBUTIONS

642 Conceptualization, A.J.M., B.K., K.H., and S.z.O.-K.; Software, S.z.O.-K.; Formal
643 Analysis, L.R. and S.z.O.-K.; Data Curation, L.R., Ll.R., and S.z.O.-K.; Methodology,
644 S.z.O.-K.; Investigation, L.R., Ll.R., and S.z.O.-K.; Writing – Original Draft, K.H., L.R.,
645 and S.z.O.-K.; Writing – Review & Editing, A.J.M., B.K., K.H., L.R., Ll.R., and S.z.O.-K.;

Visualization, L.R. and S.z.O.-K.; Funding Acquisition, A.J.M., B.K., and K.H.; Resources, A.E., A.J.M., and N.G.B.; Supervision, A.J.M., B.K., and K.H.

ACKNOWLEDGMENTS

No conflict of interest is declared.

REFERENCES

Andronov, L., Orlov, I., Lutz, Y., Vonesch, J.L., and Klaholz, B.P. (2016). ClusterViSu, a method for clustering of protein complexes by Voronoi tessellation in super-resolution microscopy. Sci. Rep. **6**:24084. 10.1038/srep24084.

Axelrod, D., Koppel, D.E., Schlessinger, J., Elson, E., and Webb, W.W. (1976). Mobility Measurement by Analysis of Fluorescence Photobleaching Recovery Kinetics. Biophys. J. **16**:1055-1069. 10.1016/S0006-3495(76)85755-4.

Bayle, V., Fiche, J.B., Burny, C., Platre, M.P., Nollmann, M., Martiniere, A., and Jaillais, Y. (2021). Single-particle tracking photoactivated localization microscopy of membrane proteins in living plant tissues. Nat. Protoc. **16**:1600-+. 10.1038/s41596-020-00471-4.

Betzig, E., Patterson, G.H., Sougrat, R., Lindwasser, O.W., Olenych, S., Bonifacino, J.S., Davidson, M.W., Lippincott-Schwartz, J., and Hess, H.F. (2006). Imaging intracellular fluorescent proteins at nanometer resolution. Science **313**:1642-1645. 10.1126/science.1127344.

Binder, A., Lambert, J., Morbitzer, R., Popp, C., Ott, T., Lahaye, T., and Parniske, M. (2014). A modular plasmid assembly kit for multigene expression, gene silencing and silencing rescue in plants. PLoS One **9**:e88218. 10.1371/journal.pone.0088218.

Caesar, K., Elgass, K., Chen, Z., Huppenberger, P., Witthoft, J., Schleifenbaum, F., Blatt, M.R., Oecking, C., and Harter, K. (2011). A fast brassinolide-regulated response pathway in the plasma membrane of Arabidopsis thaliana. Plant J. **66**:528-540. 10.1111/j.1365-313X.2011.04510.x.

Chenouard, N., Smal, I., de Chaumont, F., Maska, M., Sbalzarini, I.F., Gong, Y.H., Cardinale, J., Carthel, C., Coraluppi, S., Winter, M., et al. (2014). Objective comparison of particle tracking methods. Nat. Methods **11**:281-U247. 10.1038/nmeth.2808.

Ester, M., Kriegel, H.-P., Sander, J., and Xu, X. (1996). A density-based algorithm for discovering clusters in large spatial databases with noise. Proceedings of the Second International Conference on Knowledge Discovery and Data Mining:226–231.

Freese, N.H., Norris, D.C., and Loraine, A.E. (2016). Integrated genome browser: visual analytics platform for genomics. Bioinformatics **32**:2089-2095. 10.1093/bioinformatics/btw069.

Glöckner, N., zur Oven-Krockhaus, S., Rohr, L., Wackenhut, F., Burmeister, M., Wanke, F., Holzwart, E., Meixner, A.J., Wolf, S., and Harter, K. (2022). Three-Fluorophore FRET Enables the Analysis of Ternary Protein Association in Living Plant Cells. Plants **11**10.3390/plants11192630.

Gomez, B.G., Holzwart, E., Shi, C., Lozano-Duran, R., and Wolf, S. (2021). Phosphorylation-dependent routing of RLP44 towards brassinosteroid or phytosulfokine signalling. J. Cell Sci. **134**10.1242/jcs.259134.

Gou, X., and Li, J. (2020). Paired Receptor and Coreceptor Kinases Perceive Extracellular Signals to Control Plant Development. Plant Physiol. **182**:1667-1681. 10.1104/pp.19.01343.

Gronnier, J., Legrand, A., Loquet, A., Habenstein, B., Germain, V., and Mongrand, S. (2019). Mechanisms governing subcompartmentalization of biological membranes. Curr. Opin. Plant Biol. **52**:114-123. 10.1016/j.pbi.2019.08.003.

Gronnier, J., Crowet, J.M., Habenstein, B., Nasir, M.N., Bayle, V., Hosy, E., Platre, M.P., Gouguet, P., Raffaele, S., Martinez, D., et al. (2017). Structural basis for plant plasma membrane protein dynamics and organization into functional nanodomains. eLife **6**10.7554/eLife.26404.

Grosseholz, R., Wanke, F., Rohr, L., Glöckner, N., Rausch, L., Scholl, S., Scacchi, E., Spazierer, A.J., Shabala, L., Shabala, S., et al. (2022). Computational modeling and quantitative physiology reveal central parameters for brassinosteroid-regulated early cell physiological processes linked to elongation growth of the Arabidopsis root. eLife **11**10.7554/eLife.73031.

Hecker, A., Brand, L.H., Peter, S., Simoncello, N., Kilian, J., Harter, K., Gaudin, V., and Wanke, D. (2015). The Arabidopsis GAGA-Binding Factor BASIC PENTACYSTEINE6 Recruits the POLYCOMB-REPRESSIVE COMPLEX1 Component LIKE HETEROCHROMATIN PROTEIN1 to GAGA DNA Motifs. Plant Physiol. **168**:1013-1024. 10.1104/pp.15.00409.

Hess, S.T., Girirajan, T.P.K., and Mason, M.D. (2006). Ultra-high resolution imaging by fluorescence photoactivation localization microscopy. Biophys. J. **91**:4258-4272. 10.1529/biophysj.106.091116.

Holzwart, E., Huerta, A.I., Glockner, N., Garnelo Gomez, B., Wanke, F., Augustin, S., Askani, J.C., Schurholz, A.K., Harter, K., and Wolf, S. (2018). BRI1 controls vascular cell fate in the Arabidopsis root through RLP44 and phytosulfokine signaling. Proc. Natl. Acad. Sci. U.S.A. **115**:11838-11843. 10.1073/pnas.1814434115.

Hosy, E., Martiniere, A., Choquet, D., Maurel, C., and Luu, D.T. (2015). Super-resolved and dynamic imaging of membrane proteins in plant cells reveal contrasting kinetic profiles and multiple confinement mechanisms. Mol. Plant **8**:339-342. 10.1016/j.molp.2014.10.006.

Jaillais, Y., and Ott, T. (2020). The Nanoscale Organization of the Plasma Membrane and Its Importance in Signaling: A Proteolipid Perspective(1)([OPEN]). Plant Physiol. **182**:1682-1696. 10.1104/pp.19.01349.

Konopka, C.A., and Bednarek, S.Y. (2008). Variable-angle epifluorescence microscopy: a new way to look at protein dynamics in the plant cell cortex. Plant J. **53**:186-196. 10.1111/j.1365-313X.2007.03306.x.

Ladwig, F., Dahlke, R.I., Stuhrwohldt, N., Hartmann, J., Harter, K., and Sauter, M. (2015). Phytosulfokine Regulates Growth in Arabidopsis through a Response Module at the Plasma Membrane That Includes CYCLIC NUCLEOTIDE-GATED CHANNEL17, H+-ATPase, and BAK1. Plant Cell **27**:1718-1729. 10.1105/tpc.15.00306.

Lelek, M., Gyparaki, M.T., Beliu, G., Schueder, F., Griffie, J., Manley, S., Jungmann, R., Sauer, M., Lakadamyali, M., and Zimmer, C. (2022). Single-molecule localization microscopy (vol 1, 39, 2021). Nat. Rev. Methods Primers **2**10.1038/s43586-022-00161-3.

Levet, F., Hosy, E., Kechkar, A., Butler, C., Beghin, A., Choquet, D., and Sibarita, J.B. (2015). SR-Tesseler: a method to segment and quantify localization-based super-resolution microscopy data. Nat. Methods **12**:1065-1071. 10.1038/nmeth.3579.

Magde, D., Webb, W.W., and Elson, E. (1972). Thermodynamic Fluctuations in a Reacting System - Measurement by Fluorescence Correlation Spectroscopy. Phys. Rev. Lett. **29**:705-&. DOI 10.1103/PhysRevLett.29.705.

Manley, S., Gillette, J.M., Patterson, G.H., Shroff, H., Hess, H.F., Betzig, E., and Lippincott-Schwartz, J. (2008). High-density mapping of single-molecule trajectories

743 with photoactivated localization microscopy. Nat. Methods **5**:155-157.
744 10.1038/Nmeth.1176.

745 **Manzo, C., and Garcia-Parajo, M.F.** (2015). A review of progress in single particle
746 tracking: from methods to biophysical insights. Rep. Prog. Phys. **78**10.1088/0034-
747 4885/78/12/124601.

748 **Martiniere, A., and Zelazny, E.** (2021). Membrane nanodomains and transport
749 functions in plant. Plant Physiol. **187**:1839-1855. 10.1093/plphys/kiab312.

750 **Martiniere, A., Fiche, J.B., Smokvarska, M., Mari, S., Alcon, C., Dumont, X.,**
751 **Hematy, K., Jaillais, Y., Nollmann, M., and Maurel, C.** (2019). Osmotic Stress
752 Activates Two Reactive Oxygen Species Pathways with Distinct Effects on Protein
753 Nanodomains and Diffusion. Plant Physiol. **179**:1581-1593. 10.1104/pp.18.01065.

754 **Martiniere, A., Lavagi, I., Nageswaran, G., Rolfe, D.J., Maneta-Peyret, L., Luu,**
755 **D.T., Botchway, S.W., Webb, S.E., Mongrand, S., Maurel, C., et al.** (2012). Cell wall
756 constrains lateral diffusion of plant plasma-membrane proteins. Proc. Natl. Acad. Sci.
757 U.S.A. **109**:12805-12810. 10.1073/pnas.1202040109.

758 **McKenna, J.F., Rolfe, D.J., Webb, S.E.D., Tolmie, A.F., Botchway, S.W., Martin-**
759 **Fernandez, M.L., Hawes, C., and Runions, J.** (2019). The cell wall regulates
760 dynamics and size of plasma-membrane nanodomains in Arabidopsis. Proc. Natl.
761 Acad. Sci. U.S.A. **116**:12857-12862. 10.1073/pnas.1819077116.

762 **McKinney, S.A., Murphy, C.S., Hazelwood, K.L., Davidson, M.W., and Looger, L.L.**
763 (2009). A bright and photostable photoconvertible fluorescent protein. Nat. Methods
764 **6**:131-133. 10.1038/Nmeth.1296.

765 **Mora-Garcia, S., Vert, G., Yin, Y., Cano-Delgado, A., Cheong, H., and Chory, J.**
766 (2004). Nuclear protein phosphatases with Kelch-repeat domains modulate the
767 response to brassinosteroids in Arabidopsis. Genes Dev. **18**:448-460.
768 10.1101/gad.1174204.

769 **Nieves, D.J., Pike, J.A., Levet, F., Williamson, D.J., Baragilly, M., Oloketuyi, S., de**
770 **Marco, A., Griffie, J., Sage, D., Cohen, E.A.K., et al.** (2023). A framework for
771 evaluating the performance of SMLM cluster analysis algorithms. Nat. Methods
772 **20**:259-+. 10.1038/s41592-022-01750-6.

773 **Patterson, G.H., and Lippincott-Schwartz, J.** (2002). A photoactivatable GFP for
774 selective photolabeling of proteins and cells. Science **297**:1873-1877. DOI
775 10.1126/science.1074952.

Perraki, A., Gronnier, J., Gouguet, P., Boudsocq, M., Deroubaix, A.F., Simon, V., German-Retana, S., Legrand, A., Habenstein, B., Zipfel, C., et al. (2018). REM1.3's phospho-status defines its plasma membrane nanodomain organization and activity in restricting PVX cell-to-cell movement. PLoS Pathog. **14**:e1007378. 10.1371/journal.ppat.1007378.

Peters, R., Peters, J., and Tews, K.H. (1974). Microfluorimetric Studies on Translational Diffusion of Proteins in Erythrocyte-Membrane. Pflugers Arch. - Eur. J. Physiol. **347**:R36-R36.

Qian, H., Sheetz, M.P., and Elson, E.L. (1991). Single-Particle Tracking - Analysis of Diffusion and Flow in 2-Dimensional Systems. Biophys. J. **60**:910-921. Doi 10.1016/S0006-3495(91)82125-7.

Ries, J. (2020). SMAP: a modular super-resolution microscopy analysis platform for SMLM data. Nat. Methods **17**:870-872. 10.1038/s41592-020-0938-1.

Sage, D., Pham, T.A., Babcock, H., Lukes, T., Pengo, T., Chao, J., Velmurugan, R., Herbert, A., Agrawal, A., Colabrese, S., et al. (2019). Super-resolution fight club: assessment of 2D and 3D single-molecule localization microscopy software (vol 16, pg 387, 2019). Nat. Methods **16**:561-561. 10.1038/s41592-019-0453-4.

Saxton, M.J., and Jacobson, K. (1997). Single-particle tracking: Applications to membrane dynamics. Annu. Rev. Biophys. Biomol. Struct. **26**:373-399. DOI 10.1146/annurev.biophys.26.1.373.

Smokvarska, M., Bayle, V., Maneta-Peyret, L., Fouillen, L., Poitout, A., Dongois, A., Fiche, J.B., Gronnier, J., Garcia, J., Hofte, H., et al. (2023). The receptor kinase FERONIA regulates phosphatidylserine localization at the cell surface to modulate ROP signaling. Sci. Adv. **9**10.1126/sciadv.add4791.

Subach, F.V., Patterson, G.H., Renz, M., Lippincott-Schwartz, J., and Verkhusha, V.V. (2010). Bright Monomeric Photoactivatable Red Fluorescent Protein for Two-Color Super-Resolution sptPALM of Live Cells. J. Am. Chem. Soc. **132**:6481-6491. 10.1021/ja100906g.

Tinevez, J.-Y. (2011). simpletracker. https://github.com/tinevez/simpletracker.

Tinevez, J.Y., Perry, N., Schindelin, J., Hoopes, G.M., Reynolds, G.D., Laplantine, E., Bednarek, S.Y., Shorte, S.L., and Eliceiri, K.W. (2017). TrackMate: An open and extensible platform for single-particle tracking. Methods **115**:80-90. 10.1016/j.ymeth.2016.09.016.

Tokunaga, M., Imamoto, N., and Sakata-Sogawa, K. (2008). Highly inclined thin illumination enables clear single-molecule imaging in cells (vol 5, pg 159, 2008). Nat. Methods **5**:455-455. DOI 10.1038/nmeth0508-455.

Vert, G., and Chory, J. (2006). Downstream nuclear events in brassinosteroid signalling. Nature **441**:96-100. 10.1038/nature04681.

Wallis, T.P., Jiang, A., Young, K., Hou, H., Kudo, K., McCann, A.J., Durisic, N., Joensuu, M., Oelz, D., Nguyen, H., et al. (2023). Super-resolved trajectory-derived nanoclustering analysis using spatiotemporal indexing. Nat. Commun. **14**:3353. 10.1038/s41467-023-38866-y.

Wilkinson, M.D., Dumontier, M., Aalbersberg, I.J., Appleton, G., Axton, M., Baak, A., Blomberg, N., Boiten, J.W., Santos, L.B.D., Bourne, P.E., et al. (2016). Comment: The FAIR Guiding Principles for scientific data management and stewardship. Sci. Data **3**10.1038/sdata.2016.18.

Witthöft, J., Caesar, K., Elgass, K., Huppenberger, P., Kilian, J., Schleifenbaum, F., Oecking, C., and Harter, K. (2011). The activation of the Arabidopsis P-ATPase 1 by the brassinosteroid receptor BRI1 is independent of threonine 948 phosphorylation. Plant Signaling Behav. **6**:1063-1066. 10.4161/psb.6.7.15650.

Wolf, S. (2020). Deviating from the Beaten Track: New Twists in Brassinosteroid Receptor Function. Int. J. Mol. Sci. **21**10.3390/ijms21051561.

Wolf, S., Mravec, J., Greiner, S., Mouille, G., and Hofte, H. (2012). Plant cell wall homeostasis is mediated by brassinosteroid feedback signaling. Curr. Biol. **22**:1732-1737. 10.1016/j.cub.2012.07.036.

Wolf, S., van der Does, D., Ladwig, F., Sticht, C., Kolbeck, A., Schurholz, A.K., Augustin, S., Keinath, N., Rausch, T., Greiner, S., et al. (2014). A receptor-like protein mediates the response to pectin modification by activating brassinosteroid signaling. Proc. Natl. Acad. Sci. U.S.A. **111**:15261-15266. 10.1073/pnas.1322979111.

Yin, Y., Vafeados, D., Tao, Y., Yoshida, S., Asami, T., and Chory, J. (2005). A new class of transcription factors mediates brassinosteroid-regulated gene expression in Arabidopsis. Cell **120**:249-259. 10.1016/j.cell.2004.11.044.

Zhang, M.S., Chang, H., Zhang, Y.D., Yu, J.W., Wu, L.J., Ji, W., Chen, J.J., Liu, B., Lu, J.Z., Liu, Y.F., et al. (2012). Rational design of true monomeric and bright photoactivatable fluorescent proteins. Nat. Methods **9**:727-U297. 10.1038/Nmeth.2021.

842 **Zhang, X., Henriques, R., Lin, S.S., Niu, Q.W., and Chua, N.H.** (2006).
843 Agrobacterium-mediated transformation of Arabidopsis thaliana using the floral dip
844 method. Nat. Protoc. **1**:641-646. 10.1038/nprot.2006.97.

845 **Zhu, J.Y., Li, Y., Cao, D.M., Yang, H., Oh, E., Bi, Y., Zhu, S., and Wang, Z.Y.** (2017).
846 The F-box Protein KIB1 Mediates Brassinosteroid-Induced Inactivation and
847 Degradation of GSK3-like Kinases in Arabidopsis. Mol. Cell **66**:648-657 e644.
848 10.1016/j.molcel.2017.05.012.

849